

Rheological Behavior of Portland Clinker-Calcium Sulphoaluminate Clinker-Anhydrite Ternary Blend

Tingjie Huang, Ph.D student

School of Civil Engineering, National Engineering Laboratory for High Speed Railway Construction,
Central South University, Changsha 410075, China
Email: huangtj@csu.edu.cn, Tel: +86 15608461125

Baiyuan Li, Master student

School of Civil Engineering, National Engineering Laboratory for High Speed Railway Construction,
Central South University, Changsha 410075, China
Email: Libaiyun@csu.edu.cn

*Qiang Yuan, Ph.D, Professor, Corresponding author

School of Civil Engineering, National Engineering Laboratory for High Speed Railway Construction,
Central South University, Changsha 410075, China
Email: Yuanqiang@csu.edu.cn, Tel: +86 13548955591

Zhenguo Shi, Ph. D,

Laboratory for Concrete & Construction Chemistry, Swiss Federal Laboratories for Materials Science and
Technology (Empa), 8600 Dübendorf, Switzerland
Email: zhenguo.shi@empa.ch

Youjun Xie, Ph.D, Professor

School of Civil Engineering, National Engineering Laboratory for High Speed Railway Construction,
Central South University, Changsha 410075, China
Email: xiejy@csu.edu.cn

Caijun Shi, Ph.D. Proferssor

Key Laboratory for Green & Advanced Civil Engineering Materials and Application Technology of Hunan
Province, College of Civil Engineering, HunanUniversity, Changsha, 410082, China
Email: cshi@hnu.edu.cn

Abstract

In this paper, the rheological behavior of blended cements consisting of calcium sulfoaluminate clinker (CSA), ordinary Portland clinker (OPC) and anhydrite ($\text{C}\bar{\text{S}}$) were investigated. The shear stress-shear rate curves of OPC-CSA- $\text{C}\bar{\text{S}}$ blends with different OPC/CSA/ $\text{C}\bar{\text{S}}$ ratios were analyzed. Several rheological models were used to fit the rheological curves of cement pastes. The evolution of static yield stress was also monitored to evaluate the structural build-up rate of the blends. Besides, zeta potential measurement, calorimetric test, XRD and TGA analysis were carried out to reveal the physico-chemical kinetics of the rheological evolution of fresh blends. It was found that not only CSH gel but crystals of AFt and gypsum formed at the early age make contributions to the rheological parameters, i.e. plastic viscosity, yield stress and structural build-up.

Keywords:

Ordinary Portland cement, Calcium sulfoaluminate cement, Anhydrite, Physico-chemical kinetics, Rheology

1. Introduction

Blends of ordinary Portland cement (OPC) and calcium sulfoaluminate (CSA) cement are expected to combine advantages of these two cements and control specific properties of each, such as shrinkage of OPC-based material, expansion of CSA-based material and their setting time [1-9].

Binary systems of OPC-CSA or ternary systems mixed with various calcium sulfates (dihydrate, hemihydrate and anhydrite) have been well investigated, including the mechanical properties, the

microstructure [10, 11] and hydration process [12-14]. The ratio between the cements and the amount of calcium sulfate available in the system determines to a great extent the properties of composite systems. The setting time of OPC can be shortened by adding CSA, and the higher addition of CSA is, the shorter setting time is [15, 16]. Moreover, the composition of the OPC and the type of sulphates can considerably vary it [14, 15]. Higher CSA cement content increased crystallization stress, which lead to more expansion-induced cracks, larger porosity, weaker tensile strength and smaller dynamic modulus [1]. The increase of CSA increased the compressive strength of blends at high OPC/CSA mass ratio, but decreased the strength at low OPC/CSA [10~12].

A lot of researches indicated that the mixing of these two cements promoted early silicate and aluminate hydration [12, 13, 18]. They reacted very fast and AFt was formed within the first 5 min by the reaction between Ye'elimite (i.e., $C_4A_3\bar{S}$, the main component of the CSA clinker) and the calcium sulphates. Subsequently $C_2A\bar{S}H_8$ and CSH were formed due to the reaction of C_3S at early period [13]. In case of OPC, the addition level of calcium sulphate should be optimized considering the content and reactivity of C_3A , which leads to the formation of AFt at early age [17, 19]. However, calcium sulfate ion pairs are expected to adsorb onto tricalcium aluminate and reduce the overall reaction rate of OPC [20, 21]. In case of CSA cement, calcium sulphate content controls the formation rate and the amount of AFt, affects the AFt/AFm ratio and the water demand to achieve complete hydration [22, 23]. For ternary blend, high calcium sulphate content increases AFt contents at early age, although it does not strongly influence the hydrate assemblage of the ternary binders at late period [13].

In addition to the properties of hardened cement-based materials, the favorable rheological property at

fresh stage is also of significance, it affects the construction quality of casting and forming process and also the properties of hardened concrete [24]. Particularly, in some advanced construction technologies, such as concrete 3D printing, smart casting and formless construction [25~27], the rheology of cement-based materials should make a balance between flowability before deposition and rate of structural build-up at rest [28]. CSA was applied to improve the shape holding capacity and enhance early strength of 3D printing OPC paste [29] and OPC-based self-levelling screed [30].

The chemical composition and physical characteristics of cement greatly influence its rheological properties. Mork et al. [31] noted that the yield stress and plastic viscosity of OPC paste increased with SO_3 content. Dils et al. [32] pointed out that the OPC paste with high C_3A content, and lower SO_3 content performed the worst rheological properties. García-Maté et al. [33] believed that the SO_3 content did not present an important effect on the plastic viscosity of fresh CSA cement paste.

Recently, more and more attention has been focused on a time-dependent rheological parameter (i.e., the structural build-up rate) of cement-based material, which is due to the physical interactions between particles and the hydration of cement at early age [34, 35]. The structural build-up is responsible for the increase of static yield stress and storage modulus of cement-based materials over time [36, 37]. A high build-up rate leads to a sufficient strength to sustain the weight of subsequent casting layers, as well as ensure strong bond between cast layers [38~40]. Furthermore, fast structural build-up rate can lead to high resistance of segregation and bleeding that can improve the quality of interface between aggregate and cement paste [41,42]. This directly affects the permeability, bond to steel and mechanical properties [43]. The structural build-up rate of ordinary Portland cement-based materials

67 can be optimized by incorporating mineral admixtures [44~47], clays [48~52] and chemical additives
68 [53].

69

70 Hydration kinetics plays an important role on structural build-up of cement-based material [34]. With
71 the hydration of Portland cement particles going on, the precipitation of CSH gel on the surface of
72 particles bridges the particles. It was considered as the main origin of structural build-up [35].
73 Therefore, the requirement of rheological properties of cement-based material leads to the new
74 challenges of controlling the hydration at very early age. Hydration kinetics must be delayed to avoid
75 setting during conveying and casting, but accelerated substantially after placing in the position in order
76 to obtain the quick structuration [27, 28].

77

78 Although there are some studies on the rheological properties of Portland cement with CSA cement,
79 the rheological properties of binary binder are affected by many factors, such as the type and content
80 of calcium sulfate, the compositions of Portland cement and CSA cement. These are not well addressed
81 in literature. By using three pure minerals, i.e. clinker of Portland cement, clinker of CSA and calcium
82 sulfate, the rheological properties of binary binder of CSA and Portland can be studied in more details.
83 The objective of the present study is to characterize the rheological behaviors of ternary blends
84 composed of OPC clinker, CSA clinker and anhydrite. The influence of anhydrite dosage and of the
85 OPC/CSA mass ratio on the instantaneous and time-dependent rheological parameters were studied.
86 In order to provide more insightful evidence of rheology, zeta potential test was used to measure the
87 electro-kinetic parameters, calorimetric test was conducted to evaluate the hydration reaction of
88 cement paste, and X-ray diffraction and thermogravimetric analysis were employed to characterize the

hydrates formed during rheological test period. Hopefully, this study can provide useful information for designing a new binder with adopted rheological and setting behaviors.

91

92 2. Experimental

93 2.1 Materials and sample preparation

94 The raw materials used in this study to prepare the composite cements were ordinary Portland cement clinker and calcium sulphotoaluminate clinker and anhydrite ($C\bar{S}$). In the following, OPC refers to ordinary Portland cement clinker and CSA refers to calcium sulphotoaluminate clinker. All the raw materials were supplied by China Building Materials Academy[®]. The chemical compositions and physical properties of the OPC, CSA and $C\bar{S}$ are presented in Table 1. Their particle size distributions are shown in Fig. 1.

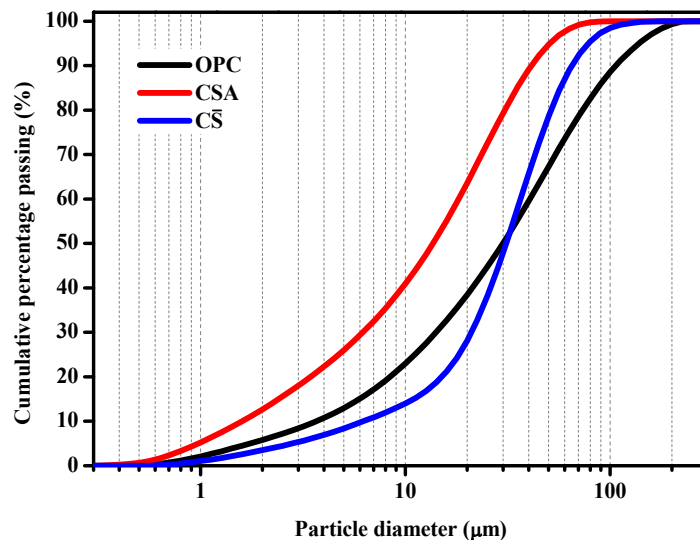


Fig. 1. Particle size distributions of powder materials

100

101 The mix proportions of the studied OPC-CSA- $C\bar{S}$ systems are given in Table 2. The influence of the
 102 OPC/CSA mass ratio was investigated at certain $C\bar{S}$ content. Two $C\bar{S}$ contents (5% and 10%) were
 103 employed to check the influence of the calcium sulphate content on the hydration mechanism and

rheological behaviors of the composite cements. The water-to-powder (w/p) ratio of 0.5 was used to prepare the paste samples. Water was first added into the Hobart N50 mixer, followed by adding the powders. The mixture was first mixed at 60 rpm for 60 s, and then stopped and the paste sample was manually homogenized for 30 s, followed by mixing at 120 rpm for 90 s, and then at 60 rpm for 30 s.

Table 1 Chemical compositions and physical properties of cementitious materials

	OPC	CSA	C \bar{S}
SiO ₂ (%)	20.76	11.72	3.03
Al ₂ O ₃ (%)	4.58	22.83	0.59
Fe ₂ O ₃ (%)	3.27	1.50	0.29
CaO (%)	62.13	46.79	39.53
MgO (%)	3.13	1.72	0.68
SO ₃ (%)	2.8	12.09	54.62
Other minor oxides	1.21	2.02	0.69
Loss on ignition (%)	2.12	1.33	0.57
Density (g/cm ³)	3.14	2.81	2.97
Blaine(cm ² /g)	2845	3770	3840

Table 2 Mix proportions of the OPC-CSA- C \bar{S} systems under investigation

Sample	Mass fraction (wt.%)			OPC/CS A mass ratio	Solid volume fraction (%)	Sample	Mass fraction (wt.%)			OPC/CS A mass ratio	Solid volume fraction (%)
	OPC	CSA	C \bar{S}				OPC	CSA	C \bar{S}		
5-10/0	95	0	5	10/0*	38.98	10-10/0	90	0	10	10/0*	39.05
5-9/1	85.5	9.5	5	9/1	39.24	10-9/1	81	9	10	9/1	39.30
5-8/8	76	19	5	8/2	39.50	10-8/8	72	18	10	8/2	39.54
5-7/3	66.5	28.5	5	7/3	39.76	10-7/3	63	27	10	7/3	39.79
5-6/4	57	38	5	6/4	40.02	10-6/4	54	36	10	6/4	40.03
5-5/5	47.5	47.5	5	5/5	40.27	10-5/5	45	45	10	5/5	40.27
5-4/6	38	57	5	4/6	40.53	10-4/6	36	54	10	4/6	40.51
5-3/7	28.5	66.5	5	3/7	40.78	10-3/7	27	63	10	3/7	40.75
5-2/8	19	76	5	2/8	41.02	10-2/8	18	72	10	2/8	40.98
5-1/9	9.5	85.5	5	1/9	41.27	10-1/9	9	81	10	1/9	41.22
5-0/10	0	95	5	0/10*	41.51	10-0/10	0	90	10	0/10*	41.45

Note: *: Binary blend, OPC+ C \bar{S} blend or CSA+C \bar{S} blend, 5-9/1 denotes 5% C \bar{S} in the powder with 90% OPC and 10%.

2.2 Rheological test

Anton paar Rheolab QC rheometer was used for rheological test. The type of rotator was CC39 with a diameter of 4.000 cm, and the inner diameter of the cylinder was 4.194 cm. In order to minimize the slip, the surfaces of the container and rotator which are in contact with cement paste were sandblasted. After mixing, the paste was immediately poured into the cylinder. Two batches of mixtures were prepared for both dynamic test and static test.

2.2.1 Dynamic test

Dynamic yield stress test was started at 5 min after the contact of cement and water, and the test was conducted as follows: pre-shear the paste at 100 s^{-1} for 60 s, then stop for 15 s, followed by linearly increasing shear rate from 0 to 100 s^{-1} within 60 s.

In order to choose the best model to characterize the dynamic rheological behavior of the different blends, four common models (Eq. 1~4) were used to fit descending curve of shear rate from 20 s^{-1} to 100 s^{-1} respectively and calculate rheological parameters.

Bingham (B) model:

$$\tau = \tau_0 + \mu \dot{\gamma} \quad (1)$$

Modified Bingham (MB) model:

$$\tau = \tau_0 + \mu \dot{\gamma} + c \dot{\gamma}^2 \quad (2)$$

Herschl-Bulkley (H-B) model:

$$\tau = \tau_0 + K \dot{\gamma}^n \quad (3)$$

Casson (C) model:

$$\tau = \tau_0 + \eta_{\infty} \dot{\gamma} + 2(\tau_0 \eta_{\infty})^{1/2} \dot{\gamma}^{1/2} \quad (4)$$

where τ_0 is dynamic yield stress, μ is apparent viscosity, c is the second order parameter in $\text{Pa}\cdot\text{s}^2$, K is consistency index, n is non-Newton index and η_{∞} is infinite viscosity.

2.2.2 Static test

For static test, a thin layer of oil was dropped on the surface of the sample to prevent the evaporation of water after pouring the sample into cylinder. The paste was at rest until specific testing time (10~45 min), static yield stress test was performed by constant shearing paste at 0.005 s^{-1} for 60 s to reach steady state [37]. The peak value of shear stress measured during this period was recorded as the static yield stress. For each resting time a new sample was employed. Since the capacity of shearing force of the equipment was 450 Pa, some samples reached the limit before 45 min, and the test was stopped. During the entire test, the temperature of the sample was maintained at $25 \text{ }^{\circ}\text{C}$ by water bath.

In this study, the model (see in Eq. 5) proposed by Perrot et al. [54] was employed to fit the data of static yield stress τ_s . The parameter A_{thix} was introduced to characterize the structural build-up rate of plain and composite cement paste. The higher A_{thix} reflects faster structural build-up of cement paste [76].

$$\tau_0(t) = \tau_{0,0} + A_{\text{thix}} t_c \left(e^{\frac{t_{\text{rest}}}{t_c}} - 1 \right) \quad (5)$$

where t_c is a characteristic time, the value of which is adjusted to obtain the best fit with experimental values.

2.3 Zeta potential measurement

159 The zeta potential was measured using the “ZetaProbe” equipment based on the electroacoustic
160 technique. A diluted blend was made for zeta potential measurement. The w/p ratio was 5. The mix
161 proportion of samples were the same to those in rheological test, as shown in Table 2. OPC, CSA, C \bar{S}
162 and distilled water were mixed in a mixer for 2 min at 300 rpm. About 300 ml of the paste was poured
163 in the sample cell of ZetaProbe. During the test, the samples were kept stirring at a speed of 300 rpm
164 so that a uniform cement suspension passes through the electrodes of the cell. The zeta potential, pH
165 value and the conductivity of the cement solution were measured every 20s and Debye length was
166 calculated automatically by the apparatus [55].

167

168 **2.4 Calorimetric test**

169 **2.4.1 Test procedure**

170 TAM Air thermal activity micro-calorimeter was used to measure the hydration heat of the blended
171 cements. The twin-chamber testing channel is the typical characteristics of this apparatus, and one
172 contains the distilled water and the other contains the predetermined amount of paste. The mixing
173 program was the same as rheological test. After mixing, the paste was immediately transferred into the
174 apparatus. During the test, the ambient temperature around the samples were maintained at 25 °C. The
175 test started at 6 min after mixing the blended cements with water. The data were recorded every 10 s.

176

177 **2.4.2 Calculation of hydration kinetic parameters**

178 The boundary nucleation and growth (BNG) model [56] has shown some advantages to describe the
179 hydration kinetics of Portland cement [57] and calcium sulphotoaluminate cement [58]. In this model,
180 the rates of nucleation and growth are assumed to be constant throughout the whole hydration process,

and the nucleation of hydrates occurs randomly on the surface of cement particles.

According to BNG model, the volume fraction of hydrates ($X(t)$) at a given time was used to estimate the degree of hydration $\alpha(t)$, which can be expressed as Eq. 6 [57~62].

$$\alpha(t) = X(t) = 1 - \exp \left\{ -S \int_0^{Gt} \left[1 - \exp \left(-\frac{\pi N}{3} G^2 t^3 \left(1 - \frac{3y^2}{G^2 t^2} + \frac{2y^3}{G^3 t^3} \right) \right) \right] dy \right\} \quad (6)$$

$$S = \frac{\text{Blaine specific surface area of particles}}{\text{density of particles}} \quad (7)$$

where S is the value of surface area for the solid particles per unit volume (μm^{-1}) and calculated by Eq. 7, G is the growth rate of nuclei ($\mu\text{m}/\text{h}$), N is the formation rate of nuclei ($\mu\text{m}^{-2}\text{h}^{-1}$) and y is a dummy variable. The degree of hydration $\alpha(t)$ is estimated by calorimetric test using Eq. 8.

$$\alpha(t) = \frac{Q(t)}{Q_{\max}} \quad (8)$$

Q_{\max} is the total heat released from the hydration of cementitious materials as measured by calorimetric test.

The formation rate of nuclei (N) and its growth rate (G) are both dominant parameters controlling the early hydration. Because the nuclei growth is anisotropic, the rate of tangent direction was defined as gG . Additionally, a parameter p was proposed to describe the proportion of growth rate inside and outside grain [56]. By further defining $\mu=y/(Gt)$, Eq. 6 can be written as Eq. 9:

$$X(t) = 1 - \exp \left\{ -2pSGt \int_0^1 \left[1 - \exp \left(-\frac{\pi N}{3} gG^2 t^3 (1 - \mu)^2 (1 + 2\mu) \right) \right] d\mu \right\}, \mu < 1 \quad (9)$$

Two independent rate constants k_N and k_G were proposed to describe the kinetics of a boundary-nucleated process (Eq. 10 and 11).

$$k_N = \pi g G^2 N / 3 \quad (10)$$

$$k_G = p S G \quad (11)$$

According to refs. [56, 57], $1/k_G$ was defined as the time for hydration products reaching the radius of “reaction vessel”. $1/(K_N)^{1/3}$ was the time needed for part of hydration products along the boundary of cement particles to become unity. Thus, the $X(t)$ can be expressed as follows (Eq. 12).

$$X(t) = 1 - \exp \left\{ - 2k_G t \int_0^1 [1 - \exp(-k_N t^3 (1 - \mu)^2 (1 + 2\mu))] d\mu \right\}, \mu < 1 \quad (12)$$

According to the literature [57], the BNG model fits well the calorimetric data, and the heat flow can be defined as $A(dx/dt)$, where A is the scaling parameter. The measured heat flow data, in particular the data between the minimum in the induction period and the second peak, were used to determine K_N and K_G values.

2.5 Solid phase Analysis

2.5.2 X-ray diffraction analysis

After mixing of the blended materials, the fresh paste was placed on a glass microscope slide and set at X-ray diffractometer at 25°C. The XRD measurements started at 15 min and 30 min after the contact of cement and water. X-ray diffraction analyses was carried out at 25 °C with a Bruker D8 Advance diffractometer (Cu K α radiation, 45mA, 35kV) with a Super speed detector, in the 2θ range 5~35°, with a scanning step size of 6° 2θ /min (total measurement time of 5 min). The crystalline phases were analyzed using the EVA software.

2.5.3 Thermogravimetric analysis

The hydration of the blend was stopped before thermogravimetric analysis (TGA). 5 grams of the sample after hydration of 10, 20, 30 and 45 min was ground with 100 ml of acetone to fine powder in an agate mortar prior to stopping hydration. The ground samples were filtrated with a Whatman filter (90 mm diameter with a pore size of 2.5 μm) and a Teflon support. The samples were washed twice with acetone and finally washed with diethyl ether [63]. The resulting samples were stored in a desiccator to avoid further hydration and any possible carbonation.

TGA was carried out with a TGA 2(SF)-Mettler Toledo. Approximately 50 mg of the prepared powdered samples were tested from 35 $^{\circ}\text{C}$ to 950 $^{\circ}\text{C}$ at a heating rate of 10 $^{\circ}\text{C}/\text{min}$ under a N_2 atmosphere.

3 Results

3.1 Dynamic rheology

3.1.1 Rheological models of OPC-CSA- $\text{C}\bar{\text{S}}$ blend

The typical shear stress vs. shear rate flow curves of OPC-CSA- $\text{C}\bar{\text{S}}$ blends are plotted in Fig. 2. The paste shows shear thinning behavior in the measured shear rate region regardless of OPC/CSA mass ratio and $\text{C}\bar{\text{S}}$ content. In order to evaluate whether the mathematic equations are suitable for the measured data, standard deviation (SD) calculated by Eq. 12 was adopted to compare the compliance of various rheological models and shear stress–shear rate data. In Eq. 12, y_{mea} is measured shear stress, y_{pre} is the predicted value by the rheological models. The results are shown in Table 3.

$$\text{SD} = \sqrt{\frac{\sum_{i=1}^n (y_{\text{mea}} - y_{\text{pre}})^2}{n - 1}} \quad (12)$$

238

239 As seen in Table 3, the Herschel-Bulkley (H-B) and modified Bingham (MB) models have lower SD
240 values than Bingham (B) and Casson (C) models, particularly in case of lower OPC/CSA ratio and
241 higher \overline{CS} content. However, the H-B model has higher SD values for ternary blends with higher
242 OPC/CSA ratio and binary CSA- \overline{CS} blends than that of MB model. This means that the modified
243 Bingham model has the best fitting for shear stress-shear rate data of OPC-CSA- \overline{CS} blends.

244

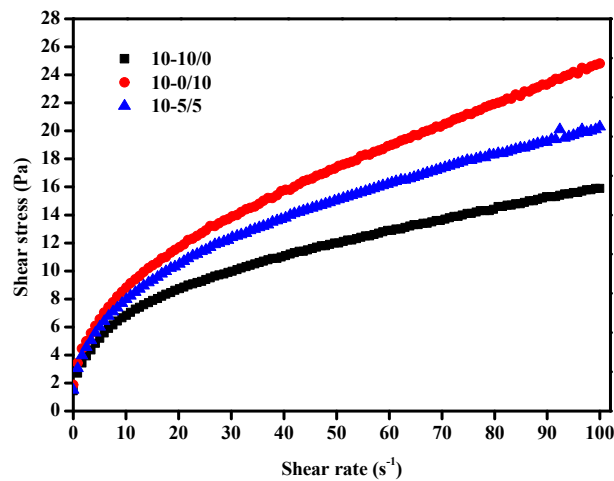


Fig. 2 Typical rheological curves of blends

245

246

Table 3 Standard deviation (SD) values for the models investigated

OPC/CSA ratio	5% \overline{CS}				10% \overline{CS}			
	B	MB	H-B	C	B	MB	H-B	C
10/0	0.1098	0.1375	0.0754	0.350	0.0901	0.090	0.1133	0.442
9/1	0.1807	0.0408	0.3135	0.461	0.1831	0.0979	0.0803	0.482
8/2	0.1174	0.0769	0.1671	0.339	0.2108	0.0822	0.0775	0.378
7/3	0.1929	0.1426	0.1441	0.515	0.1879	0.1528	0.0775	0.535
6/4	0.2285	0.0631	0.1132	0.572	0.2051	0.0785	0.1020	0.657
5/5	0.2157	0.1672	0.1151	0.494	0.2204	0.1663	0.0842	0.810
4/6	0.3098	0.1047	0.0986	0.542	0.2332	0.0936	0.0655	0.481
3/7	0.3606	0.1182	0.0787	0.418	0.2486	0.1100	0.0754	0.531
2/8	0.4795	0.1267	0.0938	0.688	0.2955	0.1318	0.0842	1.003
1/9	0.6140	0.1375	0.0931	0.763	0.3690	0.1019	0.0775	1.381
0/10	0.5230	0.0998	0.2699	0.378	0.1776	0.0696	0.0752	0.498

3.1.2 Yield stress and plastic viscosity

Yield stress and plastic viscosity are two parameters, which should be fitted to quantitatively assess the rheological behavior of the blends. Fig. 3 presents the yield stress obtained by four models. The H-B model predicts the lowest yield stress, which is one order of magnitude lower than the yield stress predicted by other rheological models. Nevertheless, the results calculated by different models shows a similar trend. It reveals that the dynamic yield stress of blend depends not only on OPC/CSA ratio, but also relates to $\text{C}\bar{\text{S}}$. Independent of the types of models used, for a given $\text{C}\bar{\text{S}}$ content, the dynamic yield stress (τ_0) of ternary composite cement paste is higher than binary OPC+ $\text{C}\bar{\text{S}}$ paste. The models predict that the τ_0 value of ternary blends is even higher than that of CSA+ $\text{C}\bar{\text{S}}$ paste. Additionally, the τ_0 value is smaller at higher OPC/CSA ratio, while the dynamic yield stresses of those with 10% $\text{C}\bar{\text{S}}$ are lower than those with 5% $\text{C}\bar{\text{S}}$ at the same OPC/CSA ratio.

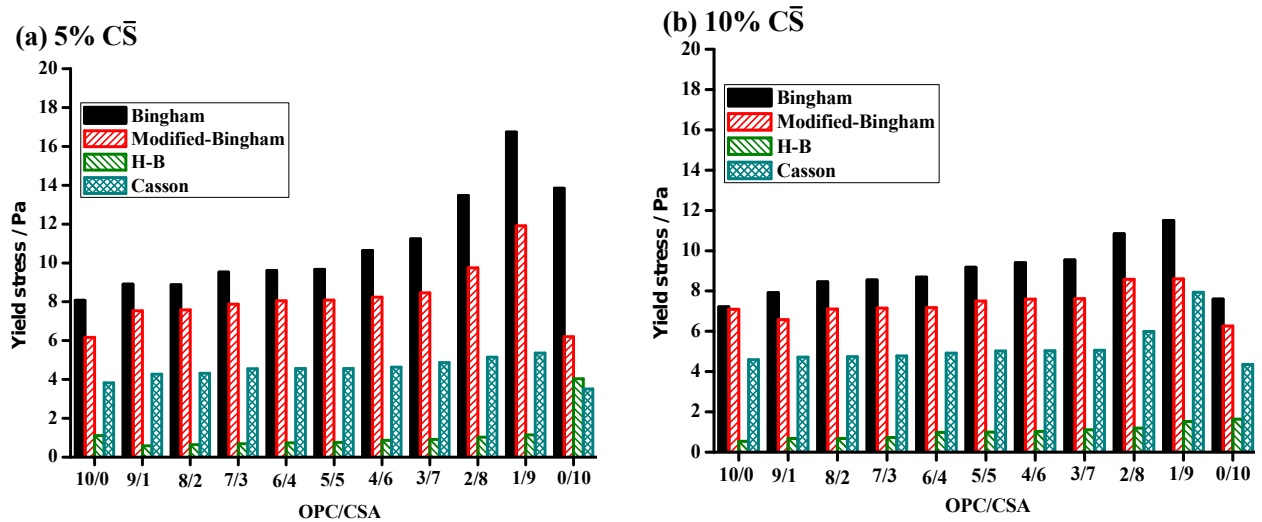


Fig. 3. The dynamic yield stress of pastes obtained by various models.

Fig. 4 shows the plastic viscosity and consistency index predicted by Bingham model and MB model. The result obtained from Bingham model is similar to that obtained from MB model at high OPC/CSA

ratio, however, the Bingham model shows higher values at lower OPC/CSA ratio. For ternary blends, the influence of OPC/CSA/C \bar{S} mass ratio on the plastic viscosity/consistency index calculated by these two models are similar. The plastic viscosity/consistency index increases both with CSA content and C \bar{S} content. Most of the plastic viscosities of ternary blends are larger than that of binary OPC+C \bar{S} and CSA + C \bar{S} pastes.

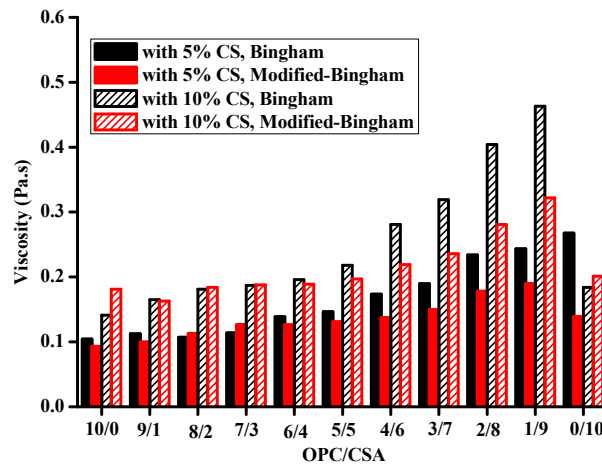


Fig. 4. The apparent viscosity of samples obtained by Bingham and Modified-Bingham

267

268 3.1.3 Shear-thinning intensity

In order to evaluate the shear-thinning intensity of the blends, the non-Newton index n was calculated based on the H-B model as summarized in Table 4. It can be observed that all of the n values of blends are less than 1, which means that all of them exhibit shear-thinning behavior [64]. The lower n value indicates a higher intensity of shear-thinning when $n < 1$ [64]. The results show that with the addition of C \bar{S} the shear-thinning intensity is increased for the OPC paste, but decreased for the CSA paste. The result also shows that the shear-thinning intensity of ternary OPC-CSA-C \bar{S} blend is enhanced with increasing the C \bar{S} content. However, the highest shear-thinning intensity is obtained for the blends when the OPC content is close to CSA content (in this study, the highest shearing-thinning intensity is observed at OPC/CSA=6/4 or 5/5, when the content of C \bar{S} is 5% or 10%).

278

279 In summary, the initial rheological parameter of cement pastes with ternary OPC-CSA-C \bar{S} system
 280 depends not only on OPC/CSA ratio, but also on the content of C \bar{S} . The decrease of the OPC/CSA
 281 ratio leads to a higher yield stress and a higher plastic viscosity. However, increasing the percentage
 282 of C \bar{S} in ternary system results in a lower dynamic yield stress but a higher plastic viscosity and a
 283 higher shear-thinning intensity.

284

Table 4 The non-Newton index of sample obtained by H-B model

OPC/CSA ratio	5% C \bar{S}	10% C \bar{S}
10/0	0.420	0.450
9/1	0.440	0.449
8/2	0.420	0.445
7/3	0.411	0.429
6/4	0.389	0.435
5/5	0.389	0.410
4/6	0.387	0.442
3/7	0.390	0.420
2/8	0.402	0.505
1/9	0.440	0.601
0/10	0.736	0.427

285

286 3.2 Electro-kinetic characteristics

287 [Table 5](#) shows the average values of electro-kinetic parameters (zeta potential, Debye length,
 288 conductivity and pH value) of C \bar{S} solution, OPC solution, CSA solution, OPC + C \bar{S} diluted blends
 289 and CSA + C \bar{S} diluted blends over 20 min. The change in zeta potential depends on either a change
 290 in surface charge or adsorption of ions to the surfaces. Debye length reflects the scope where repulsive
 291 electrostatic effect persists. Debye length relates on the ionic strength of the bulk electrolyte. The
 292 conductivity of cement solution reflects the ionic concentration and ionic conductivity. [65]

293

It can be seen that the zeta potentials (ζ) of the suspensions of $\text{C}\bar{\text{S}}$, OPC, CSA are all positive, the value of OPC solution is the largest while that of CSA solution is the smallest and close to zero. Although 5% $\text{C}\bar{\text{S}}$ content shortens the Debye length of OPC solution and CSA solution while 10% $\text{C}\bar{\text{S}}$ content enlarges the value of Debye length, the influence of $\text{C}\bar{\text{S}}$ in zeta potential values of OPC solution and CSA solution differs. In case of OPC+ $\text{C}\bar{\text{S}}$ binary blend, the increase in $\text{C}\bar{\text{S}}$ content decreases the zeta potential. Conversely, in case of CSA+ $\text{C}\bar{\text{S}}$ blend, larger proportion of $\text{C}\bar{\text{S}}$ leads to higher ζ value.

The average electro-kinetic parameters of OPC-CSA- $\text{C}\bar{\text{S}}$ blends are also listed in Table 6. The result notes that except for sample 5-3/7, the zeta potentials of ternary blends are positive, the increase of CSA content reduces ζ value of blends. For blends with 5% $\text{C}\bar{\text{S}}$, increasing CSA content decreases the conductivity and pH value. The lower conductivity and pH value reflect the less dissolved ions stemming from blend. It may contribute to lower value of ionic strength. Thus, Debye length increases. For blends with 10% $\text{C}\bar{\text{S}}$, the conductivity and pH value decrease with the CSA content when OPC/CSA is larger than 4/6, but it turns to increase with CSA content at the lowers. The Debye length of blends with 10% $\text{C}\bar{\text{S}}$ thus shows an opposite trend. Furthermore, the increase of $\text{C}\bar{\text{S}}$ content results in the increase of Debye length and leads to the increases of zeta potential.

Therefore, larger CSA content in ternary system results in longer Debye length but lower zeta potential, while higher proportion of $\text{C}\bar{\text{S}}$ contributes to larger value of Debye length and higher and zeta potential.

Table 5 Electro-kinetic parameters of diluted $\text{C}\bar{\text{S}}$, OPC, CSA paste and their binary blends

Samples	ζ (mV)	Debye length (nm)	Conductivity (mS/cm)	pH value
Only $\text{C}\bar{\text{S}}$	2.31	1.61	5.33	6.89

Only OPC	3.13	1.25	8.06	13.09
5-10/0	2.40	1.12	10.05	12.82
10-10/0	2.16	1.92	3.44	12.56
Only CSA	0.47	2.70	1.74	12.41
5-0/10	0.46	1.54	5.33	12.31
10-0/10	2.13	3.70	0.94	12.48

Table 6 Electro-kinetic parameters of diluted OPC-CSA-C \bar{S} pastes

OPC/CS A mass ratio	5% C \bar{S}				10% C \bar{S}			
	ζ (mV)	Debye length (nm)	Conductivity (mS/cm)	pH value	ζ (mV)	Debye length (nm)	Conductivity (mS/cm)	pH value
9/1	2.14	1.19	8.92	12.93	4.46	2.44	2.48	12.87
8/2	2.46	1.19	8.97	12.67	3.52	2.78	2.60	12.57
7/3	1.62	1.33	7.08	12.29	2.87	2.86	2.51	12.44
6/4	1.63	1.35	6.82	12.11	2.45	3.03	2.39	12.28
5/5	1.12	1.44	5.99	12.16	1.82	3.13	2.27	12.43
4/6	0.45	1.64	4.67	12.01	1.35	3.45	2.07	12.29
3/7	-0.23	1.89	3.52	11.95	0.72	2.45	2.18	12.17
2/8	0.39	1.95	2.68	12.02	0.66	2.59	2.94	12.06
1/9	0.47	2.03	2.34	11.88	0.63	2.45	2.46	12.14

3.3 Evolution of static yield stress with resting time

The static yield stress vs. resting time curves of OPC pastes and CSA cement paste with different contents of C \bar{S} were given in Fig. 5. Perrot's model was employed to fit these data and the result is given in Table 7. The result shows that the C \bar{S} influences the static yield stress of the OPC paste and CSA cement paste differently. For the OPC pastes, 5% of C \bar{S} reduces the initial yield stress $\tau_{0,0}$, while the $\tau_{0,0}$ is higher when the dosage of C \bar{S} is 10%. After longer resting time, the increase of yield stress at 10% C \bar{S} is indicating a significant increase of setting time. On the contrary, the incorporation of C \bar{S} significantly increases not only the $\tau_{0,0}$ value but also the structural build-up rate A_{thix} of CSA cement paste comparing to the sample without C \bar{S} . However, no difference in A_{thix} value of CSA cement paste is observed between samples with 5% and 10% C \bar{S} .

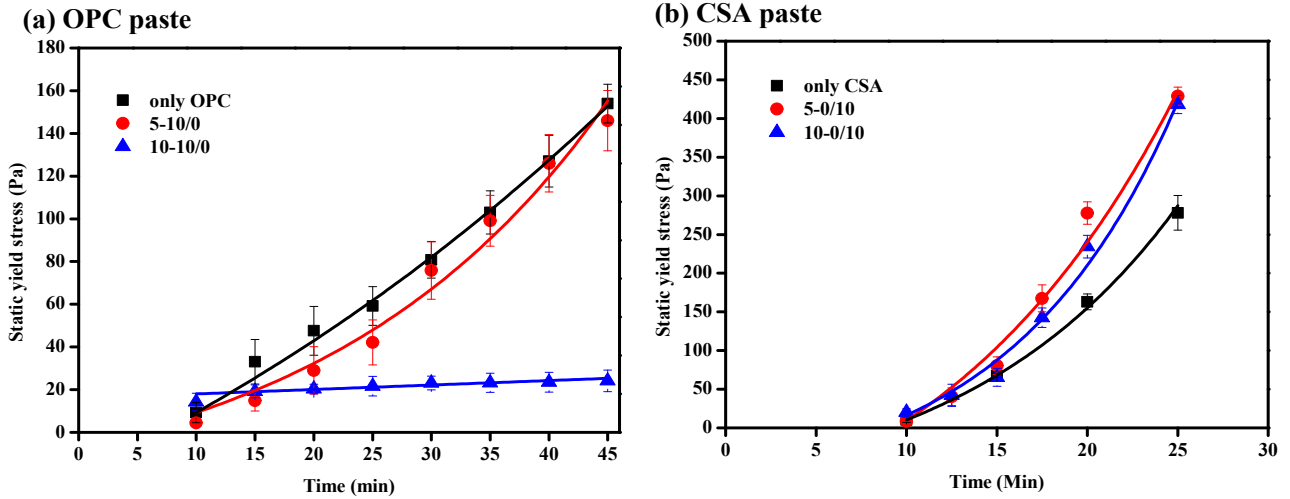


Fig. 5 The influence of $\bar{C}\bar{S}$ on the evolution of static yield stress of OPC and CSA paste with resting time

Table 7 Effect of $\bar{C}\bar{S}$ content on the structural build-up parameters of OPC paste and CSA paste obtained from Perrot model

Samples	$\tau_{0,0}$ (Pa)	A_{thix} (Pa/min)	t_c (min)	R^2
Only OPC	9.65	3.118	66.488	0.9966
5-10/0	7.73	1.860	24.237	0.9663
10-10/0	14.01	0.209	1249.089	0.9293
Only CSA	6.142	9.306	12.072	0.9925
5-0/10	9.202	15.450	14.915	0.9875
10-0/10	11.256	14.709	9.182	0.9821

Fig. 6 plots the evolution curves of static yield stress of ternary OPC-CSA- $\bar{C}\bar{S}$ blends. The structural build-up rate was calculated by Perrot's model as well. The results are listed in Table 8. It shows a well fit between Perrot's model and experimental data of ternary blends. As can be seen in Table 8, the proportions of OPC, CSA and $\bar{C}\bar{S}$ affects the structural build-up of blends greatly. The initial yield stress $\tau_{0,0}$ of blends is increased with the CSA content and $\bar{C}\bar{S}$ content. The higher CSA proportion is of benefit for structuration of blends. However, at the same OPC/CSA ratio, A_{thix} value of those with 10% $\bar{C}\bar{S}$ is always higher than that of those with 5% $\bar{C}\bar{S}$. Particularly, when OPC/CSA ratio is lower

339 than 6/4, the structural build-up rates of blends containing 10% CS have quadrupled in that of blends
 340 with 5% CS . It reveals that the higher percentage of CS conduces to structural build-up of ternary
 341 blends, which is contrary to the result for CSA cement paste and OPC paste. It should be noted that
 342 when the OPC/CSA ratio drops to 1/9, the A_{thix} of ternary composite cement paste with 5% CS is over
 343 that of binary CSA+ CS paste; and for 10% of CS content, the build-up rate of the blend with only
 344 7/3 of OPC/CSA ratio is already quicker than that of CSA+ CS paste.
 345
 346 Therefore, the increase of CSA content accelerates the structural build-up of ternary blends at rest. The
 347 incorporation of CS is in favor of the re-structuration of ternary blends, and it becomes more
 348 significantly when CSA dominates.

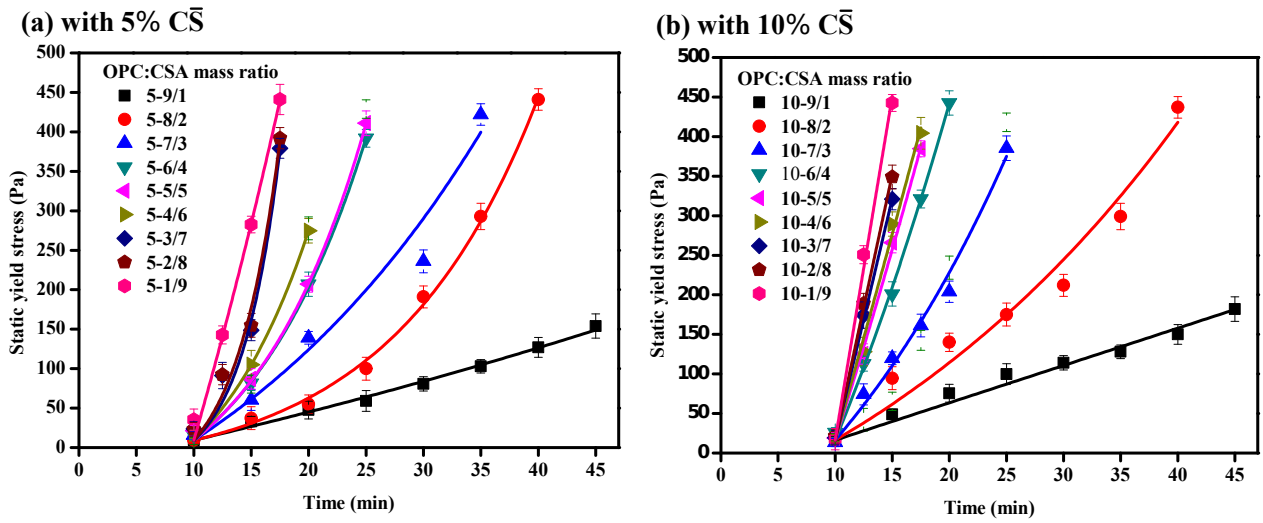


Fig. 6 Effect of OPC/CSA mass ratio on structural build-up of blends

354

355

Table 8 The structural build-up parameters of OPC-CSA-C \bar{S} pastes obtained from Perrot's model

OPC/CSA mass ratio	5% C \bar{S}				10% C \bar{S}			
	$\tau_{0,0}$ (Pa)	A_{thix} (Pa/min)	t_c (min)	R^2	$\tau_{0,0}$ (Pa)	A_{thix} (Pa/min)	t_c (min)	R^2
9/1	9.273	3.506	12.579	0.9982	16.069	4.723	15.707	0.9810
8/2	8.911	9.499	27.069	0.9696	17.116	8.456	34.938	0.9793
7/3	9.014	11.703	10.709	0.9980	16.055	16.831	9.182	0.9921
6/4	9.421	11.649	10.120	0.9925	16.921	35.290	27.356	0.9961
5/5	9.252	13.329	10.071	0.9974	16.859	46.051	55.143	0.9983
4/6	9.433	14.217	8.759	0.9804	17.021	51.176	133.363	0.9950
3/7	9.625	16.360	3.390	0.9794	17.152	61.136	213.814	0.9989
2/8	10.752	16.392	3.385	0.9760	18.044	67.226	119.159	0.9974
1/9	12.564	50.503	30.010	0.9856	20.210	87.001	108.182	0.9908

356

357

3.4 Hydration kinetics and phase changes

358

3.4.1 Hydration heat

359

Calorimetric testing results of OPC-CSA-C \bar{S} blends are given in Fig. 7. As can be seen in the figure,

360

the hydration of OPC+ C \bar{S} paste is still in the induction period when it is subjected to the rheology

361

test. The higher percentage of C \bar{S} slightly retards the induction period and reduces the heat releasing

362

rate in that period. In contrast, there is no obvious induction period for the CSA+ C \bar{S} paste, whereas

363

the rheology test period is within the accelerating period of hydration. During the rheology test period,

364

the heat flow value of CSA+ 10% C \bar{S} is significantly higher than CSA+ 5% C \bar{S} paste. The main peak

365

of heat flow of CSA+ 10% C \bar{S} blend occurs earlier than that of the blend with 5% C \bar{S} . It is agreed

366

with Refs. [13, 14] that the existence of C \bar{S} accelerates the hydration of CSA, but it delays the

367

hydration of OPC.

368

369

For the ternary OPC-CSA-C \bar{S} systems, the hydration heat is influenced by OPC/CSA ratio as well as

370 $C\bar{S}$ content. When OPC is blended with CSA, it becomes more difficult to distinguish the induction
371 period and the accelerating period, particularly at higher OPC/CSA ratio. The decrease of OPC/CSA
372 ratio makes the main peak (i.e. silicate reaction [13]) occur earlier and causes a higher heat releasing
373 rate during rheology test. When $C\bar{S}$ content is 5% and OPC/CSA ratio drops to 6/4 or lower, the heat
374 flow value including peak value of ternary pastes outnumbers the CSA+ $C\bar{S}$, and accelerating period is
375 also shortened. However, the larger $C\bar{S}$ proportion performs an opposite effect. It reduces the heat
376 flow values and delays the peak occurrence.

377

378 According to calorimetric data, it can be concluded that the higher CSA content is, the more rapid
379 reaction rate is. Moreover, $C\bar{S}$ retards the hydration of ternary system. The difference of hydration
380 heat releasing rate reveals the difference of hydrates kinetics in cement pastes.

381

382 Based on the assumption that the rates of nucleation and growth are constant throughout the whole
383 hydration process [57, 58, 60], the hydration kinetics of cement paste during structural build-up period
384 can be investigated. Hydration kinetic parameters obtained by BNG model are listed in [Table 9](#).

385 According to Ref. [34], nucleation constant K_N describes the rate of covering the surface of cement
386 particles with hydration products in unit volume of paste and growth constant K_G indicates the rate of
387 filling the pore space between particles in unit volume of paste. [Table 9](#) suggests that high CSA content
388 results in considerable enhancements in the nucleation and growth rates. The K_G value of ternary
389 blends is significantly higher than that of the OPC+ $C\bar{S}$ paste. Overall, an increasing trend on K_G of
390 ternary paste is observed with reducing the OPC/CSA ratio. The K_G value of the ternary blends is
391 higher compared to the value of CSA+ $C\bar{S}$ paste when OPC/CSA ratio is decreased to 2/8.

392

393 Moreover, the K_N value of ternary blends is also higher than that of OPC+ $C\bar{S}$ paste. The K_N value is
394 improved by more than an order of magnitude at higher CSA content. When the proportion of CSA is
395 more than 60% of composite cement, the K_N value is even larger than that of CSA+ $C\bar{S}$ paste.

396

397 As shown in [Table 9](#), the K_G value of OPC+ $C\bar{S}$ blend remains nearly unchanged with the increase of
398 $C\bar{S}$ content, however, the K_N value decreases. In contrast, the K_N and K_G values of CSA cement system
399 are both increased at higher $C\bar{S}$ content. However, the effect of $C\bar{S}$ content on the hydration kinetics
400 of ternary OPC+CSA+ $C\bar{S}$ system depends on the OPC/CSA ratio. When OPC/CSA ratio is greater
401 than 8/2, the K_G values of those with 5% $C\bar{S}$ are higher than that of those with 10% $C\bar{S}$. Opposite
402 result is observed when the OPC/CSA value is lower than 8/2. When the content of OPC is larger than
403 the content of CSA, the K_N values of blends with 5% $C\bar{S}$ is greater than that of those with 5% $C\bar{S}$.
404 However, the former is smaller than the later when CSA dominates.

405

406 The results of hydration heat flow and hydration kinetics suggest that the presence of CSA accelerates
407 the hydration evolution of ternary system, and increases the nucleation and growth kinetics of hydrates
408 at structural build-up period. The addition of $C\bar{S}$ retards the hydration of ternary system while it further
409 improves the hydration kinetics of nucleation and growth kinetics of hydrates at higher CSA content.

410

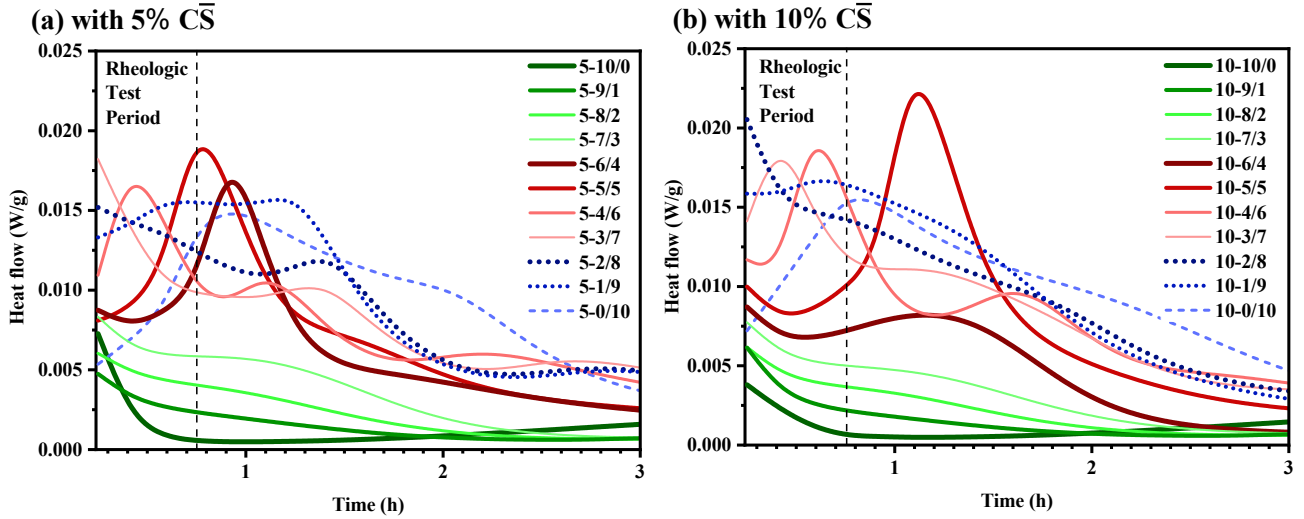


Fig. 7 Hydration heat flow of OPC-CSA- $\overline{\text{CS}}$ pastes with different compositions

Table 9 Estimated surface area of cement particles per unit volume of paste and hydration kinetic parameters obtained from BNG model

OPC/CSA mass ratio	5% $\overline{\text{CS}}$			10% $\overline{\text{CS}}$		
	S (μm^{-1})	K_G (h^{-1})	K_N $\times 10^{-3}(\text{h}^{-3})$	S (μm^{-1})	K_G (h^{-1})	K_N $\times 10^{-3}(\text{h}^{-3})$
10/0	0.9170	0.0239	0.0045	0.9363	0.0204	0.0027
9/1	0.9875	0.1338	0.0082	1.0035	0.0300	0.0037
8/2	1.0596	0.1780	0.0399	1.0721	0.1382	0.0013
7/3	1.1333	0.2238	0.0143	1.1422	0.2221	0.0065
6/4	1.2087	0.2260	3.2807	1.2139	0.2493	0.0230
5/5	1.2859	0.2362	4.2843	1.2871	0.2690	5.3107
4/6	1.3649	0.2211	4.0999	1.3619	0.2438	4.1734
3/7	1.4457	0.2125	3.1934	1.4384	0.2532	3.9167
2/8	1.5285	0.2568	3.7903	1.5167	0.3049	4.5137
1/9	1.6134	0.3001	4.7083	1.5967	0.3353	4.0898
0/10	1.7003	0.2417	3.1832	1.6786	0.2719	3.7654

3.4.2 XRD analysis and DTG results

In order to reveal the hydrates formed during the rheological test period, the XRD analysis and DTA analysis were carried out to characterize the solid phase in ternary blends during 10~30 min. Fig. 8

416 plots the XRD results of blends with different OPC/CSA ratios and $C\bar{S}$ contents at 15 min and 30 min.

417 It can be seen a very weak diffraction peak of calcium silicate hydrate occurs at 15 min in both two

418 XRD patterns of OPC+ $C\bar{S}$ pastes in addition to the strong $C\bar{S}$ peak. No significant changes in the

419 XRD patterns are observed for OPC+ $C\bar{S}$ pastes from 15 min to 30 min. Ettringite and gypsum are the

420 main hydrates formed in both CSA+ 5% $C\bar{S}$ and CSA+10% $C\bar{S}$ pastes according to XRD data. It can

421 be clearly observed that the AFt peaks become stronger with time. However, the gypsum peaks become

422 weaker from 15 min to 30 min. It can also be seen that both calcium silicate hydrate and ettringite are

423 formed in ternary OPC+ CSA+ $C\bar{S}$ pastes. The peak intensity of AFt increases with time, while the

424 intensity of the peak relates to gypsum is reduced. The influences of OPC/CSA ratio on the peak

425 intensity of ettringite and CSH are opposite. The peaks of OPC and CSA hydrates in ternary composite

426 pastes are sharper than those in OPC+ $C\bar{S}$ and CSA+ $C\bar{S}$ pastes. The lower OPC/CSA ratio results in

427 much stronger ettringite peaks while corresponding weaker CSH peaks in ternary cement pastes.

428 Furthermore, the increasing content of $C\bar{S}$ leads to sharper peaks of ettringite and CSH. This positive

429 effect of $C\bar{S}$ becomes more significant with time.

430

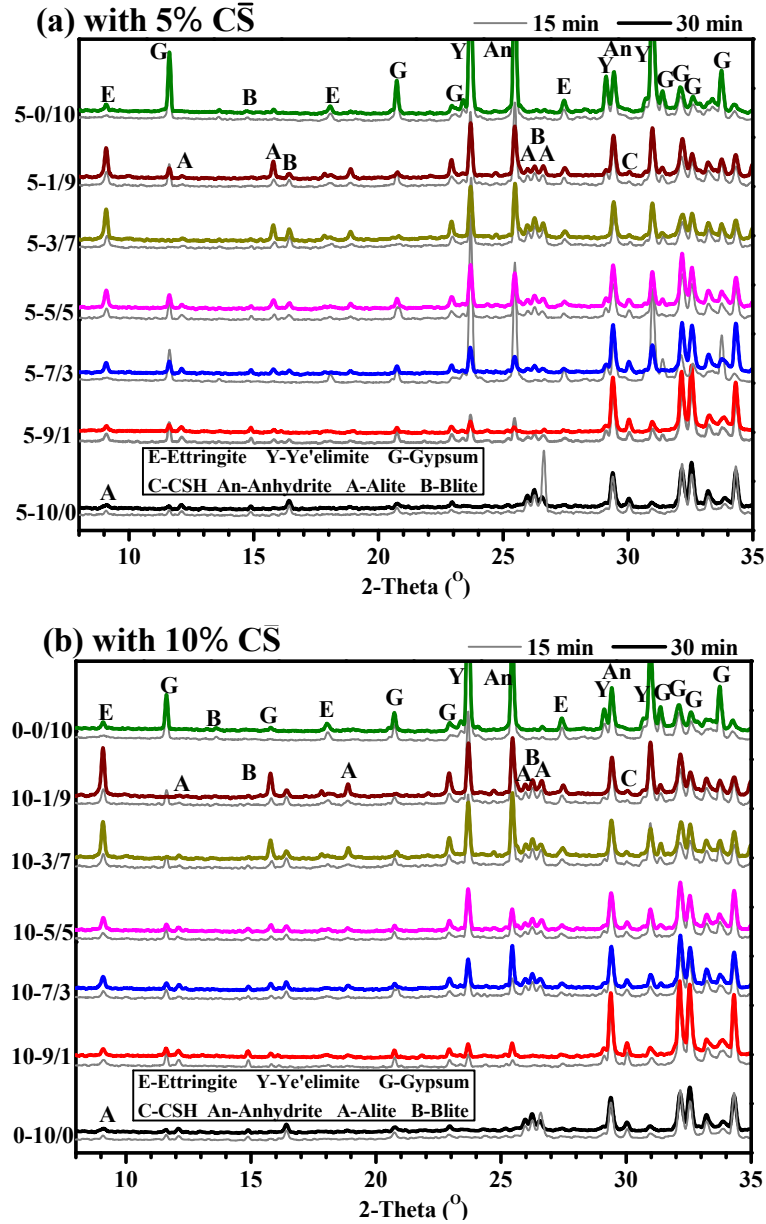


Fig. 8 The XRD patterns of OPC-CSA-C \bar{S} pastes with different compositions at 15 min (below curve) and 30 min (upper curve). E: Ettringite (PDF# 41-1451), Y: Ye'elimite (PDF# 33-0256), G: Gypsum (PDF# 33-0311), C: calcium silicate hydrate ($\text{Ca}_2\text{SiO}_4 \cdot 0.35\text{H}_2\text{O}$ [PDF# 15-0641], $\text{Ca}_2\text{SiO}_4 \cdot \text{H}_2\text{O}$ [PDF# 03-0594], $\text{Ca}_{1.5}\text{SiO}_{3.5} \cdot x\text{H}_2\text{O}$ [PDF# 33-0306]), An: Anhydrite (PDF# 37-1496), A: Alite (PDF# 49-0442), B: β -Blite (PDF# 35-0642)

431

432 The TGA analyses shown in Fig. 9 and Fig. 10 confirm the observations from XRD. Fig. 9 shows the
 433 DTG curves of the samples after 30 min of hydration. Two major peaks are observed for the OPC+ C
 434 \bar{S} blends. The weight loss between 85~95 °C is attributed to the decomposition of CSH and/or
 435 ettringite. The second peak between 100~130 °C is due to decomposition of gypsum. Similar results

are also obtained for the CSA+ $\text{C}\bar{\text{S}}$ blends, where the peak around 100 °C is mainly due to the presence of ettringite according to XRD analysis. For the OPC+CSA+ $\text{C}\bar{\text{S}}$ blends, it can be observed that two peaks present in the curves of those with high OPC/CSA ratio and lower content of $\text{C}\bar{\text{S}}$, while three peaks occur in the curves of those with low OPC/CSA ratio or high content of $\text{C}\bar{\text{S}}$. In addition to gypsum, ettringite and CSH, observed for all samples, the peak between 230~250 °C is associated with the decomposition of amorphous or micro-crystalline aluminum hydroxide (AH_3) according to the published studies [13, 66].

Moreover, it can be seen that the peak intensity for CSH/AfT and gypsum is increasing with the decrease of OPC/CSA ratio. This is attributed to the larger extent of CSH/ettringite and gypsum formation when the proportion of CSA is higher. In case of blends with 10% $\text{C}\bar{\text{S}}$, the intensity of AH_3 peak also becomes stronger with the increasing amount of CSA.

The DTG results of the samples over time are also shown in Fig. 10. It shows that the peak intensity of CSH, AfT and AH_3 increases with time for all cement blends. The peak intensity of gypsum shows an increasing trend over time for samples with 10% $\text{C}\bar{\text{S}}$, however for the samples with 5% $\text{C}\bar{\text{S}}$, no changes seem to be observed during 10~30 min. The results suggest the continuous increase on the amount of AH_3 , AfT and CSH during the rheological test period. Besides, gypsum was formed before 10 min and the amount is not increased during that period if the $\text{C}\bar{\text{S}}$ was low. It can also be observed from Fig 10 that the ternary system with 10% $\text{C}\bar{\text{S}}$ exhibits the greater peak in the range of 80~110 °C compared to system with same OPC/CSA ratio but 5% $\text{C}\bar{\text{S}}$. It confirms the XRD result that the incorporation of $\text{C}\bar{\text{S}}$ favors the formation of AfT and CSH.

458

459 In summary, the XRD and DTA results indicated that compounding OPC and CSA not only accelerates
460 the silicate reaction but also the aluminate reactions at very early hydration stage, which is in
461 agreement with the conclusion of Ref. [13]. The gypsum, CSH and AFt are formed in a ternary system
462 during the structural build-up period and the formation extent of those hydrates changes the whole
463 time. The higher amounts of CSA and anhydrate tends to form CSH and AFt, as well as gypsum.
464

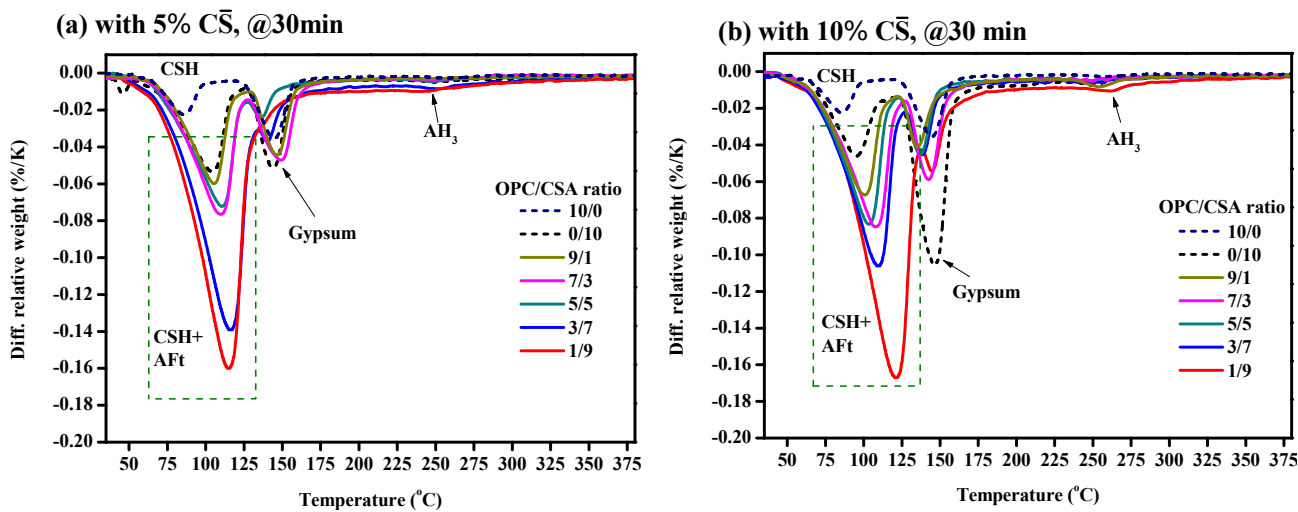
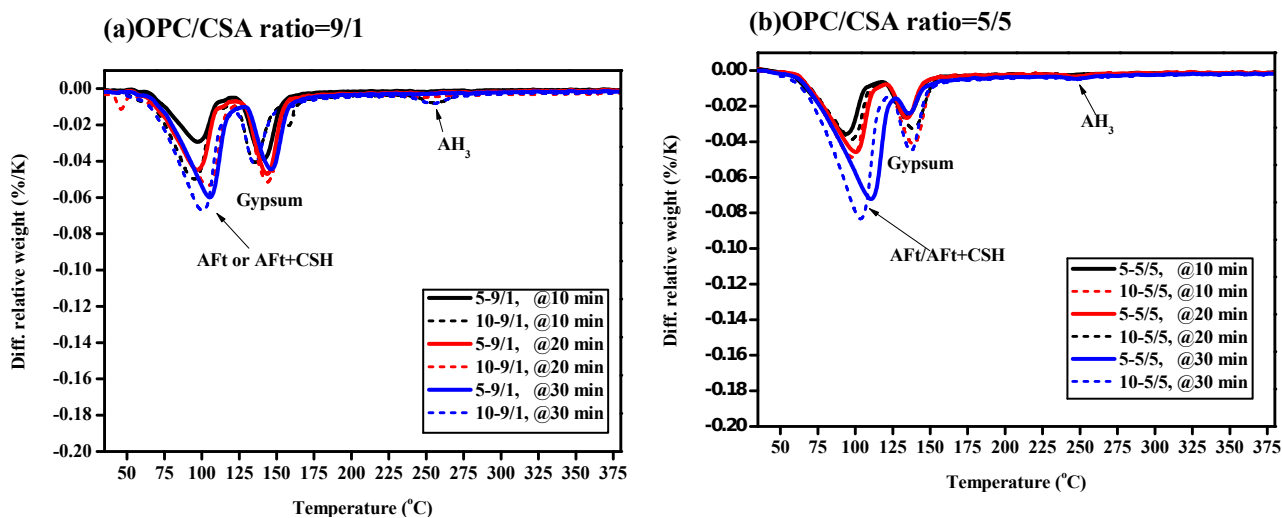


Fig. 9 The TGA plots of OPC-CSA- $\text{CS}\bar{\text{S}}$ pastes with different compositions at 30 min



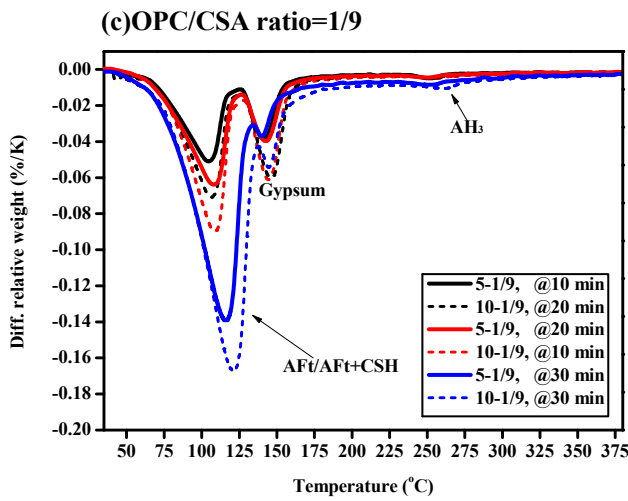


Fig. 10. The DTG data of ternary blends over time

4 Discussion

The initial and time-dependent rheological parameters of Portland clinker-calcium sulphoaluminate clinker-anhydrite blends are closely related to their relative contents. According to the present study, it has been proved that the proportion of these three components affects the electro-kinetics of blend, which determines colloidal electrostatic interaction of particles in a ternary system. Besides, the relative amounts of three components also influences the assemblage and formation rate of hydrates in the ternary system, which is mainly responsible for the structure and the rigidity of fresh cement paste. This section compares the correlation between electro-kinetics, hydration kinetics and the evolution of rheological parameters of ternary blends. It aims to discuss how the rheology of OPC-CSA-CS \bar{S} blend is controlled by the physical action and hydration.

4.1 Relationship between the initial rheological feature, electro-kinetics and hydration kinetics of OPC-CSA-CS \bar{S} ternary blend

The dynamic yield stress of cementitious materials originates from the colloidal interaction and direct

480 contact between particles [67]. It is important in quantifying flowability and is related to the slump and
481 slump flow test in field [68~70]. It was noted that the higher dynamic yield stress is, the poorer the
482 flowability is.

483

484 According to above-mentioned results, the increase of CSA content slightly increases the dynamic
485 yield stress of fresh ternary OPC-CSA-C \bar{S} blends and significantly increases their viscosity. It means
486 that enlarging CSA content causes the loss of flowability.

487

488 Initial rheological feature of fresh paste relates strongly to the solid volume fraction. As shown in
489 [Table 2](#), the increase of CSA content increases the solid volume fraction of ternary blend at constant
490 mass ratio, which is one of the reasons for increasing dynamic yield stress [71, 72]. Additionally, it
491 can be seen in Table 9, in case of ternary blends, the estimated surface area of particles per volume (S)
492 is enlarged significantly with the increase of CSA content. It also has positive effect on increasing
493 yield stress and viscosity [24, 75]. Besides, surface interactions and hydration occurring in blend also
494 should be responsible.

495

496 The surface interactions consist in a fresh blend of two opposing forces, the attractive van der Waals
497 and the repulsive electrical double layer force. The electrical double layer force is a function of the
498 square value of zeta potential (ζ^2). Namely, the larger ζ^2 is, the larger the electrical double layer force
499 is [65]. According to results shown in [section 3.2](#), the increase of CSA content reduces the ζ (ζ^2) of
500 blend, which means that the higher proportion of CSA weakens the repulsive electrical force between
501 particles in blend. It makes the attraction between charged particles become easier and the attractive

502 force become stronger [65]. When the blend is subjected to a shear force, it is more difficult to
503 overcome the interforce between particles and make them move. Thus, the dynamic yield stress
504 increases with CSA content.

505

506 As seen from Table 2 and Table 9, increasing $C\bar{S}$ content leads to little changes in the solid volume
507 fraction and the estimated surface area of particles per volume (S) of ternary blends. However, the
508 increase of $C\bar{S}$ compensates the flowability by significantly reducing the dynamic yield stress. The
509 variation of zeta potential due to the increase of $C\bar{S}$ can also explain it. According to the results, the
510 zeta potential of ternary blends with 10% $C\bar{S}$ is greater than the values of those with 5%. Moreover,
511 Debye length of the former is nearly twice as that of the latter, which is also favorable for the
512 improvement of electrostatic effect between particles [65]. It means that the larger content of $C\bar{S}$
513 increases the repulsive electrical force between particles and reduces the possibility of aggregation. It
514 is easier to break the electrostatic interaction between particles in ternary blends. Thus, $C\bar{S}$ lowers the
515 resistance of the blend to flow, which is responsible for the lower dynamic yield stress.

516

517 Kapur[73], Scales[74] and Johnson[75] believed that dynamic yield stress is negatively related to the
518 ζ^2 value of a suspension. Fig. 11 plots the relationship between the ζ^2 value and dynamic yield stress
519 of ternary blends obtained by MB model and HB model. It can be observed that the dynamic yield
520 stress of the fresh blend decreases with the increase of the ζ^2 value. In particular, the dynamic yield
521 stress data obtained by MB model presents better correlation with ζ^2 .

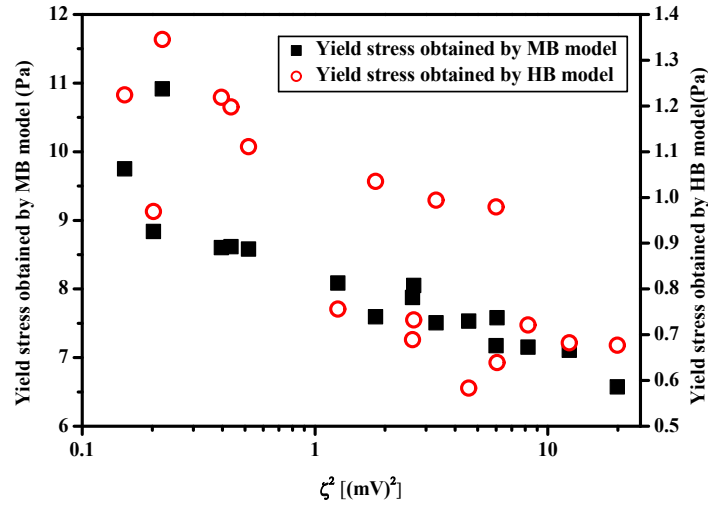


Fig. 11. The relationship between the ζ^2 value and dynamic yield stress of ternary blends

522

523 The hydration of blends can affect the surface characteristic and solid volume fraction of blends. The
 524 coarseness of surface and volume fraction can significantly influence the initial rheological feature of
 525 the blend [24].

526

527 As shown in Table 9, blend with higher CSA content has the much higher nucleation and growth
 528 kinetics of hydrate. The quick formation of needle-like AFt crystal or denser hydrates aggregate makes
 529 the surface of cement grain become coarser, which enhances the friction between neighboring particles
 530 when paste is subjected to shear force. The quicker growth of hydrate covered on the surface of
 531 particles makes it more possible to increase the solid volume fraction of blend at very early stage. The
 532 higher solid volume fraction is, the larger yield stress is.

533

534 Likewise, the negative effect of $C\bar{S}$ on dynamic yield stress is also attributed to the retarding effect of
 535 $C\bar{S}$ on hydration and its negative effect on nucleation of hydrates (see Fig. 7 and Table 9). The adverse
 536 effect of $C\bar{S}$ on hydration results in less amount of hydrates covered on the grains at very early age,

therefore particles could easily slip and pass through under shearing. Furthermore, the increase of apparent viscosity caused by the incorporation of CS is due to the higher viscosity of CS paste than that of OPC paste and CSA cement paste [77, 78].

Shear-thinning and shear-thickening are shear-induced responses, and their intensities are related to the nature of paste at the same testing program [79~81]. It relates to the interparticle force and dispersed efficiency of the system. Under the variation of shear-rate between $0\sim 100\text{ s}^{-1}$, the ternary OPC-CSA- CS blend behaves shear thinning, and the intensity increases with the content of CS and with the CSA content at higher OPC/CSA ratios. It reveals that the blends applied with a higher shear rate has a smaller size of aggregation and a lower level of flocculation. And the increase of CSA and CS makes this phenomenon more significant. The high shear rate may break the rigid “AFt linkage” between particles, untangled the interlock of hydrates and even polished the surface of cement grains. Because of the higher amount of “AFt linkage” in pastes with high CSA content, the sensitivity of the blends with high CSA content on shear rate is stronger. However, when the OPC/CSA ratio is lower, the faster growth of AFt makes the interaction of particle much stronger, which is difficult to break the aggregations. Therefore, the shear thinning intensity in this case becomes weaker.

4.2 Origin of the structural build-up of OPC-CSA- CS ternary blend

The structural build-up rate of the microstructure of fresh cement paste after casting is of importance to the multi-layer casting operations and the design of formwork [28, 41]. The structural build-up of cement suspensions is a complex phenomenon associated with the combined effect of both physical structuration due to inter-particles colloidal interactions and chemical rigidification resulting from

559 cement hydration [34, 76]. As soon as cement particles is mixed with water, the contact solution is
560 enriched with multivalent ions including cations (Ca^{2+} , K^+ , Na^+ , Al^{3+}) and anions (SO_4^{2-} , OH^-). Once
561 the bulk solution becomes saturated and causes the formation of ettringite-like compounds and the
562 precipitation of CSH on the cement surface [19]. The surface of cements and their hydration products
563 become charged either by dissociation of surface groups or adsorption of ions from the electrolyte
564 solution [82, 83]. Roussel [35] observed that this physical process takes only a few seconds. During
565 this period, the strength of the particle network is determined by the colloidal surface interactions.
566 Although these products may not yet form rigid bonds between cement particles, they do fill pore space
567 that was previously occupied by water. At a certain moment known as a percolation threshold, enough
568 particles are connected to form a continuous solid path within the fluid medium, and gradually
569 develops to a stronger skeleton. Roussel [35] attributed the rigid links between particles in OPC paste
570 in this process to metastable CSH, and named it CSH bridge. The process can take up to 100s. The
571 particle structure is further strengthened as the number and size of the hydrate bridges increase.

572

573 Differing with OPC paste, not only the ionic composition of liquid but also the hydrates and their
574 contents are significantly altered when OPC is blended with CSA. Correspondingly, both colloidal
575 surface interactions and rigid links between cement particles are changed.

576

577 In the case of ternary blend, AFt, CSH, gypsum and amorphous AH_3 are formed during the rheology
578 test period, as discussed in [section 3.4.2](#). Thus, the structure of fresh paste is developed by the
579 formation and growth of these hydrates.

580

581 Fig. 12 demonstrates the networks of interacting cement particles in the structure of ternary blends.
 582 Excluding the “CSH bridge”, there are two main linkage in the structure of paste. One is contributed
 583 by AFt crystal and another is due to the gypsum network. The morphology of AFt is generally
 584 described by prisms or needles with a high specific surface area. The formation of AFt on the surface
 585 of cement grain results in a strong friction force between interparticle. The AFt crystal outside the
 586 grains interlace with each other to establish an interspace reticulate structure in fresh paste. The
 587 gypsum is yielded in the space among cement particles. The morphology of gypsum is rod-like and
 588 the size of gypsum is an order of magnitude bigger than needle-like AFt [19]. The network formed by
 589 gypsum provided a rigid tie for cement grain, which makes the structure of blend stronger.
 590
 591 Therefore, the structural build-up of OPC-CSA-C \bar{S} ternary blends originated from the rigid links of
 592 CSH and AFt and the gypsum network, as well as colloidal surface interaction.

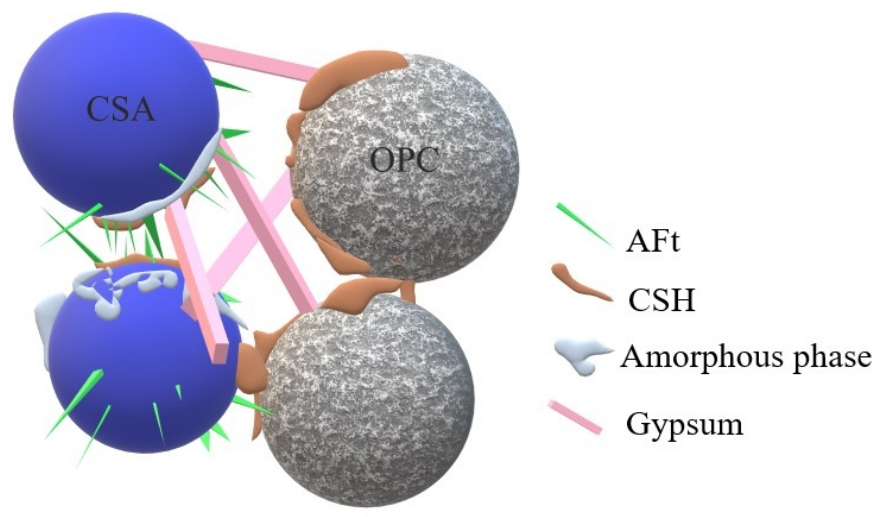


Fig. 12. Schematic drawing of the hydrates covered on the surface of cement particles and the network(s) of interacting cement particles in OPC-CSA- C \bar{S} ternary system during the dormant period.

593
 594 By comparing phase analysis results (section 3.4.2), hydration evolution and kinetics (section 3.4.1)

and the structural build-up rate (section 3.3), it suggests that the role of CSA and \overline{CS} on accelerating structural build-up is due to their positive effect on the hydration kinetics of main hydrates. The nucleation and growth kinetics of hydrates calculated from calorimetry data, shown in Table 9, is used to describe the relationship between hydration and structural build-up rate and it is a good evidence to explain the impact of the \overline{CS} and CSA.

Fig. 13 plots the structural build-up rate of blends A_{thix} value with the growth kinetics of hydrates K_G value. As the plot shows, the A_{thix} value increases with K_G value, and the curve agrees with the exponential relation. It means that the rate of filling the pore space between particles in unit volume of paste plays an important role on the structural build-up rate. And, the increase of CSA and \overline{CS} accelerate the filling rate of hydrate in the pore of initial structure, thus they speed up the structural build-up rate of blends.

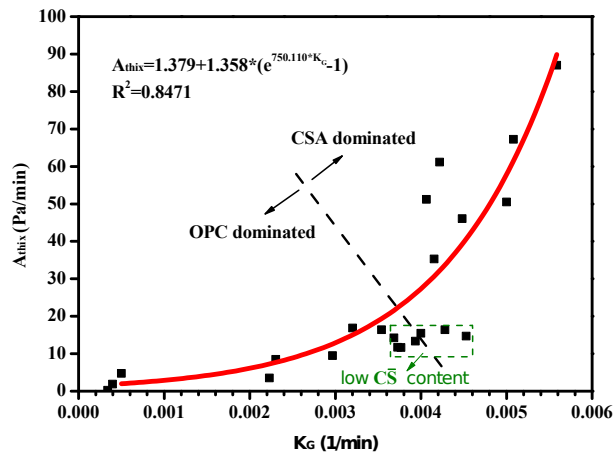


Fig. 13. The relationship between the growth kinetics of hydrates K_G and the structural build-up rate A_{thix} of ternary blends

5 Conclusions

Based on the aforementioned results and discussion, the following conclusions can be drawn:

1. The OPC-CSA- \overline{CS} blended pastes are non-Newtonian flow, and exhibit a shear thinning behavior.

Herschel-Bulkley model and modified Bingham model is suitable for calculating the rheological parameters of fresh ternary blends.

2. The rheological parameters of OPC-CSA- $\overline{\text{CS}}$ blends depend on OPC/CSA ratio and the content of $\overline{\text{CS}}$. The high content of CSA causes a higher dynamic yield stress and apparent viscosity. The increase of $\overline{\text{CS}}$ favors the flowability of blends by reducing the dynamic yield stress, although it leads to a higher apparent viscosity. $\overline{\text{CS}}$ in a ternary system improves the extent of shear thinning. Besides, the higher amount of CSA and the high proportion of $\overline{\text{CS}}$ in system collectively accelerates the structural build-up of blends. Thus, the appropriate increase of $\overline{\text{CS}}$ not only benefits flowability under casting, but also helps re-structuration at rest.

3. CSA and $\overline{\text{CS}}$ have different effects on initial rheology, while they both make positive effects on the structural build-up of blends. This may stem from the difference between their effects on electro-kinetics and hydration kinetics.

4. The initial rheology of ternary blends depends on the electro-kinetics. The dynamic yield stress of the blend relates closely with zeta potential. The increase of CSA reduces the zeta potential of blends. It results in a weak repulsive electrostatic force and a correspondingly stronger attraction between particles, which improves the dynamic yield stress. Conversely, the increase of $\overline{\text{CS}}$ enlarges the zeta potential and thus decreases the dynamic yield stress.

5. The structural build-up of blend attributes to the formation of main hydrates, including CSH, AFt

and gypsum, and their nucleation and growth kinetics. The network established by crystal with various scales and rigid bridges between particles makes a stronger structure of ternary blends. The higher growth kinetics of those hydrates is, the faster structuration rate is. The CSA and anhydrate enlarge the K_G value of hydrates, which accelerates the filling rate of hydrates in the spaces of the structure. It is responsible for their positive effect on structural build-up. Besides, the delaying action of $C\bar{S}$ on hydration process explains its desirable influence on initial flowability.

Acknowledgments

Financial supports by National Key R&D Program of China (contract No. 2017YFB0310100) and National Natural Science Foundation of China (contract No. 51778629) are greatly appreciated.

6 References

- [1] P. Chaunsali, P. Mondal, J. Bullard, Influence of Calcium Sulfphoaluminate (CSA) Cement Content on Expansion and Hydration Behavior of Various Ordinary Portland Cement-CSA Blends, *J. Am. Ceram. Soc.*, 98(2015):1-8.
- [2] I. Mehdipour, K. Khayat, Enhancing the performance of calcium sulfphoaluminate blended cements with shrinkage reducing admixture or lightweight sand, *Cem Concr Comp.* 87(2018), 29-43.
- [3] M. Polivka, C. Willson, Properties of Shrinkage-Compensating Concretes, ACI Publication No. SP-38. 227–37, 1973
- [4] A. Klein and C. Troxell, Studies of Calcium Sulfphoaluminate Admixtures or Expansive Cements, *Am. Soc. Test. Mater.*, 58(1958) 986–1008.

- 656 [5] K. Nakagawa, Y. Watanabe, I. Mino, T. Kitsuta, Adoption of Electrofused Calcium
657 Sulphoaluminate Clinker for Ultra-high Strength Concrete, Proceedings of the 6th International
658 Congress on the Chemistry of Cement (ICCC), Supplementary Paper, Section 3, URSS, Moscow,
659 1974.
- 660 [6] M. Cohen. Theories of expansion in sulphoaluminate – type expansive cements: schools of
661 thought. *Cem Concr Res*, 13(1983) 809–18.
- 662 [7] M. Ish-Shalom, A. Bentur, Properties of type K expansive cement of pure components I.
663 Hydration of unrestrained paste of expansive component results. *Cem Concr Res*, 4(1974) 519–
664 32.
- 665 [8] A. Bentur, M. Ish-Shalom, Properties of type K expansive cement of pure components II.
666 Proposed mechanism of ettringite formation and expansion in unrestrained paste of pure
667 expansive component. *Cem Concr Res*. 4(1974) 709–21.
- 668 [9] M. Ish-Shalom, A. Bentur, Properties of type K expansive cement of pure components III.
669 Hydration of pure expansive component under varying restraining conditions. *Cem Concr Res*,
670 5(1975) 139–52.
- 671 [10] I. Janotka, U. Krajčí, An experimental study on the upgrade of sulphoaluminate-belite cement
672 systems by blending with Portland cement, *Adv. Cem. Res*. 11(1999), 35-41.
- 673 [11] I. Janotka, L. Krajčí, A. Ray, S.C. Mojumdar, The hydration phase and pore structure formation
674 in the blends of sulphoaluminate-belite cement with Portland cement, *Cem Concr Res*, 33 (2003)
675 489–497
- 676 [12] R. Trauchessec, J. Mechling, A. Lecomte, A. Roux, B. Le Rolland, Hydration of ordinary
677 Portland cement and calcium sulphoaluminate cement blends, *Cem Concr Comp*. 56(2015), 106-

- [13] P. Laure, W. Frank, L. Barbara, The ternary system Portland cement–calcium sulphoaluminate clinker–anhydrite: Hydration mechanism and mortar properties, *Cem Concr Comp.* 32(2010),497-507.
- [14] L. Pelletierchaigat, F. Winnefeld, B. Lothenbach, Influence of the calcium sulphate source on the hydration mechanism of Portland cement-calcium sulphoaluminate clinker-calcium sulphate binders, *Cem Concr Comp.* 33(2011) 551-561.
- [15] D. Gastaldi, F. Canonico, L. Capelli, M. Bianchi, M. Pace, A. Telesca, Hydraulic behaviour of calcium sulphoaluminate cement alone and in mixture with Portland cement. In: *Proc. 13th int. Congr. chem. cem., Madrid, Spain; 2011*,412.
- [16] K. Kano, Quality control system and predication of strength from phase composition of very high early strength cement, *Cem Sci Concr Technol.* 52(1998), 16-21.
- [17] J. Bullard, H. Jennings, R. Livingston, Mechanisms of cement hydration, *Cem. Concr. Res.*, 41(2011):1208-1223.
- [18] P. Chaunsali, P. Mondal, Physico-chemical interaction between mineral admixtures and OPC–calcium sulphoaluminate (CSA) cements and its influence on early-age expansion, *Cem. Concr. Res.*, 80 (2016)10-20.
- [19] H. Taylor. *Cement chemistry*. London: Thomas Telford Publishing; 1997.
- [20] R. Myers, G. Geng, J. Li, E. Rodríguez, J. Ha, P. Kidkhunthod, G. Sposito, L.N. Lammers, A.P. Kirchheim, P.J.M. Monteiro, Role of adsorption phenomena in cubic tricalcium aluminate dissolution, *Langmuir.*, 33 (2017) 45–55
- [21] J. Skalny, M.E. Tadros, Retardation of Tricalcium aluminate hydration by sulfates, *J. Am. Ceram.*

700 Soc., 60 (1977), 174–175

701 [22] F. Winnefeld , S. Barlag, Calorimetric and thermogravimetric study on the influence of calcium
702 sulfate on the hydration of ye’elimite, J. Therm. Anal. Calorim., 101(2010) 949-957.

703 [23] F. Glasser, Advances in sulfphoaluminate cements. In: Proceedings 5th international symposium
704 on the cement and concrete, vol. 1; 2002. p. 14–24

705 [24] D. Jiao, C. Shi, Y. Qiang, Effect of constituents on rheological properties of fresh concrete-A
706 review, Cem Concr Comp., 83(2017) 146-159.

707 [25] D. Marchon, S. Kawashima, H. Bessaies-Bey, S. Mantellato and S. Ng, Hydration and
708 rheology control of concrete for digital fabrication: Potential admixtures and cement chemistry,
709 Cem. Concr. Res. 112 (2018), 96-110.

710 [26] L. Reiter, T. Wangler, N. Roussel and R. J. Flatt, The role of early age structural build-up in
711 digital fabrication with concrete, Cem. Concr. Res., 112 (2018), 86-95.

712 [27] D. Asprone, C. Menna, F. P. Bos, T. A. M. Salet, J. Mata-Falcón and W. Kaufmann, Rethinking
713 reinforcement for digital fabrication with concrete, Cem. Concr. Res., 112 (2018), 111-121.

714 [28] N. Roussel, Rheological requirements for printable concretes, Cem. Concr. Res., 112 (2018),
715 76-85.

716 [29] N. Khalil, G. Aouad, Use of calcium sulfphoaluminate cements for setting control of 3D-
717 printing mortars, Constr. Build. Mater., 157(2017) 382-391.

718 [30] R. Kwasny-Echterhagen, L. Amathieu, F. Estienne, Calcium Aluminate Cement: A Polyvalent
719 Blender for Various Applications in the Building Industry, Proceedings of the International
720 Conference on Dry Mixes, St. Petersburg., 2003.

721 [31] J. Mork, O. Gjörv, Effect of gypsum-hemihydrate ratio in cement on rheological properties of

722 fresh concrete, *ACI Mater. J.* 94 (2) (1997) 142~146.

723 [32] J. Dils, V. Boel, G. De Schutter, Influence of cement type and mixing pressure on air content,
724 rheology and mechanical properties of UHPC, *Constr. Build. Mater.* 41 (2013) 455~463

725 [33] M. García-Maté, I. Santacruz, Rheological and hydration characterization of calcium
726 sulphoaluminate cement pastes, *Cem Concr Comp.*, 34(2012) 684-691.

727 [34] A. Mostafa, A. Yahia, Physico-chemical kinetics of structural build-up of neat cement-based
728 suspensions, *Cem. Concr. Res.* 97 (2017) 11-27.

729 [35] N. Roussel, G. Ovarlez, S. Garrault, C. Brumaud, The origins of thixotropy of fresh cement pastes,
730 *Cem. Concr. Res.*, 42 (2012) 148–157.

731 [36] Q. Yuan, X.Lu, K.H Khayat., D. Feys, C. Shi, Small amplitude oscillatory shear technique to
732 evaluate structural build-up of cement paste, *Mater. Struct.* 50 (2017) 1-12.

733 [37] Q. Yuan, D. Zhou, K.H Khayat., D. Feys, C. Shi, On the measurement of evolution of structural
734 build-up of cement paste with time by static yield stress test vs. small amplitude oscillatory shear
735 test, *Cem. Concr. Res.*, (2017), 183-189.

736 [38] A. Perrot, A., D. Rangeard, A. Pierre, Structural built-up of cement-based materials used for 3D-
737 printing extrusion techniques, *Mater. Struct.* 49 (2016), 1213-1220

738 [39] R. Wolfs, F. Bos, T. Salet, Early age mechanical behaviour of 3D printed concrete: Numerical
739 modelling and experimental testing. *Cem. Concr. Res.*, 106 (2018), 103-116.

740 [40] T. Wangler, E. Lloret, L. Reiter, N. Hack, F. Gramazio, M. Kohler, R. Flatt, Digital concrete:
741 opportunities and challenges. *RILEM Technol. Lett.*, 1(2016), 67-75.

742 [41] J. Assaad, K. Khayat, Effect of viscosity-enhancing admixtures on formwork pressure and
743 thixotropy of self-consolidating concrete, *ACI Mater. J.*, 103 (2006) 280–287.

- 744 [42] K. Khayat, J. Assaad, Effect of w/cm and high-range water-reducing admixture on formwork
745 pressure and thixotropy of self-consolidating concrete, *ACI Mater. J.*, 103 (2006) 186–193.
- 746 [43] J. Assaad, K. Khayat, J. Daczko, Evaluation of static stability of self-consolidating concrete, *ACI*
747 *Mater. J.*, 101 (2004) 168 – 176.
- 748 [44] M. Rahman, M. Baluch, M. Malik, Thixotropic behavior of self-compacting concrete with
749 different mineral admixtures, *Constr. Build. Mater.*, 50(2014), 710-717.
- 750 [45] R. Ahari, T. Erdem, K. Ramyar, Thixotropy and structural breakdown properties of self-
751 consolidating concrete containing various supplementary cementitious materials, *Cem. Concr.*
752 *Comp.*, 59(2015), 26-37.
- 753 [46] A. Mostafa, A. Yahia, New approach to assess build-up of cement-based suspensions, *Cem.*
754 *Concr. Res.*, 85 (2016) 174–182.
- 755 [47] Q. Yuan, D. Zhou, Effect of mineral admixtures on the structural build-up of cement paste, *Constr.*
756 *Build. Mater.*, 160(2018)117-126.
- 757 [48] N. Tregger, M. Pakula, S. Shah, Influence of clays on the rheology of cement pastes, *Cem. Concr.*
758 *Res.*, 40 (2010) 384–391
- 759 [49] S. Kawashima, M. Chaouche, D. Corr, Rate of thixotropic rebuilding of cement pastes modified
760 with highly purified attapulgite clays, *Cem. Concr. Res.*, 53 (2013) 112-118.
- 761 [50] R. Ferron, A. Gregori, Z. Sun, S. Shah, Rheological method to evaluate structural buildup in self-
762 consolidating concrete cement past, *ACI Mater. J.* 104(2007) 242–50.
- 763 [51] Z. Quanji, G. Lomboy, K. Wang, Influence of nano-sized highly purified magnesium aluminosilicate
764 clay on thixotropic behavior of fresh cement pastes, *Constr. Build. Mater.*, 69 (2014) 295-
765 300.

- 766 [52] Y. Qian and G. De Schutter, Enhancing thixotropy of fresh cement pastes with nanoclay in
767 presence of polycarboxylate ether superplasticizer (PCE), *Cem. Concr. Res.*, 111 (2018), 15-22.
- 768 [53] K. Khayal, J. Assaad, Use of Thixotropy-Enhancing agent to reduce formwork pressure exerted
769 by Self-Consolidating concrete, *ACI Mater. J.*, 105 (2008) pp. 88.
- 770 [54]] A. Perrot, A. Pierre, S. Vitaloni and V. Picandet, Prediction of lateral form pressure exerted by
771 concrete at low casting rates, *Mater. Struct.* 48 (2015), 2315-2322.
- 772 [55] Electro acoustics tutorial and zeta probe operators manual, Colloidal Dynamics; 2004
- 773 [56] J. Cahn, The kinetics of grain boundary nucleated reactions, *Acta Metall.* 4 (1956) 449-459.
- 774 [57] G. Scherer, J. Zhang, J. Thomas, Nucleation and growth models for hydration of cement, *Cem.*
775 *Concr. Res.*, 42 (2012) 982-993.
- 776 [58] H. Zhou, J. Liu, hydration kinetics process of low alkalinity sulfoaluminate cement and its
777 thermodynamical properties, *Procedia Engineering*, 27(2012) 323-331.
- 778 [59] G. Artioli, J. Bullard, Cement hydration: the role of adsorption and crystal growth, *Cryst. Res.*
779 *Technol.* 48 (10) (2013) 903-918.
- 780 [60] P. Brown, L. Liberman, G. Frohnsdorff, Kinetics of the early hydration of Tricalcium aluminate
781 in solutions containing calcium sulfate, *J. Am. Ceram. Soc.* 67 (1984) 793–795.
- 782 [61] K. Scrivener, P. Juilland, P. Monteiro, Advances in understanding hydration of Portland cement,
783 Keynote Pap 14th Int Congr Chem Cem ICCC 2015, 78, Part A, 2015, pp. 38–56.
- 784 [62] L. Buffo-Lacarrière, A. Sellier, G. Escadeillas, A. Turatsinze, Multiphasic finite element
785 modeling of concrete hydration, *Cem. Concr. Res.*, 37 (2007) 131–138.
- 786 [63] J. Wang, Hydration mechanism of cements based on low-CO₂ clinkers containing belite,
787 ye'elimite and calcium alumino-ferrite. PhD Thesis University of Lille, France, 2010.

- 788 [64] F. De Larrard, C. Ferraris, T. Sedran, Fresh concrete: a Herschel-Bulkley material, *Mater. Struct.*
789 31 (7) (1998) 494–498.
- 790 [65] A. Otsuki, Coupling colloidal forces with yield stress of charged inorganic particle suspension:
791 A review, *Electrophoresis*, 39(2018) 690-701.
- 792 [66] J. Zhou, K. Zheng, Chemical effect of nano-alumina on early-age hydration of Portland cement,
793 *Cem. Concr. Res.*, 116(2019) 159-167.
- 794 [67] P. Banfill, X. Yongmot, P. Domonet, Relationship between the rheology of unvibrated fresh
795 concrete and its flow under vibration in a vertical pipe apparatus, *Mag. Concr. Res.* 51 (3) (1999)
796 181-190.
- 797 [68] N. Roussel, P. Coussot, “Fifty-cent rheometer” for yield stress measurements: from slump to
798 spreading flow, *J. Rheology*. 49 (2005) 705-718.
- 799 [69] N. Pashias, D. Boger, J. Summers, D. Glenister, A fifty cent rheometer for yield stress
800 measurement, *J. Rheology*, 40 (1996) 1179-1189
- 801 [70] A. Pierre, C. Lanos, P. Estelle, Extension of spread-slump formulae for yield stress evaluation,
802 *Appl. Rheol.* 23 (2013) 63849.
- 803 [71] R. Flatt, P. Bowen, Yield stress of multimodal powder suspensions: an extension of the YODEL
804 (yield stress model), *J. am. Ceram. Soc.* 90 (2007) 1038–1044.
- 805 [72] R. Flatt, P. Bowen, Yodel: a yield stress model for suspensions, *J. am. Ceram. Soc.*, 89 (2006)
806 1244–1256
- 807 [73] P. Kapur, P. Scales, D. Boger, Yield stress of suspensions loaded with size distributed particles,
808 *Aiche J.*, 43(1997):1171-1179.
- 809 [74] P. Scales, S. Johnson, T. Healy, Shear yield stress of partially flocculated colloidal suspensions,

- 810 Aiche J., 44(1998) 538-544.
- 811 [75] S. Johnson, G. Franks, P. Scales, Surface chemistry-rheology relationships in concentrated
812 mineral suspensions, *Int. J. Miner Process.*, 58(2000):267-304.
- 813 [76] N. Roussel, A thixotropy model for fresh fluid concretes: theory, validation and applications, *Cem.*
814 *Concr. Res.*, 36 (2006) 1797–1806.
- 815 [77] J. Peng, J. Qu, J. Zhang J, Adsorption characteristics of water-reducing agents on gypsum surface
816 and its effect on the rheology of gypsum plaster, *Cem. Concr. Res.*, 35(2005) 527-531.
- 817 [78] M. Arıkan, K. Sobolev, The optimization of a gypsum-based composite material, *Cem. Concr.*
818 *Res.*, 32(2002) 1725-1728.
- 819 [79] H. Li, F. Huang, Y. Xie, Effect of water–powder ratio on shear thickening response of SCC,
820 *Constr. Build. Mater.*, 131 (2017) 585–591.
- 821 [80] A. Yahia, Effect of solid concentration and shear rate on shear-thickening response of high-
822 performance cement suspensions, *Constr. Build. Mater.*, 53 (2014) 517–521.
- 823 [81] R. Hoffman, Discontinuous and dilatant viscosity behavior in concentrated suspensions. II.
824 Theory and experimental tests, *J. Colloid. Interface Sci.*, 46 (3) (1974) 491–506.
- 825 [82] I. Pointeau, P. Reiller, N. Mace, C. Landesman, N. Coreau. Measurement and modeling of the
826 surface potential evaluation of hydrated cement pastes as a function of degradation, *J. Colloid.*
827 *Interface Sci.*, 300 (2006), 33–44
- 828 [83] H. Viallis-Terrisse, A. Nonat, J. Petit. Zeta-Potential study of calcium silicate hydrates interacting
829 with alkaline cations, *J. Colloid. Interface Sci.*, 244(2001), 58–65.
- 830